Probabilistic Models and Fragility Estimates for Unreinforced Masonry Walls Subject to In-Plane Horizontal Forces

Leandro Iannacone   Marco Andreini   Paolo Gardoni   Mauro Sassu

Abstract: Unreinforced masonry (URM) buildings make up a significant portion of the built environment, with hollow clay being the predominant choice for the units. The capacity of URM buildings is a function of the capacity of its walls, both to vertical and horizontal forces. However, URM is particularly vulnerable to the effect of horizontal forces due to the low tensile strength of the mortar that holds the units together. URM walls are subject to significant in-plane horizontal forces during seismic events, so that a proper quantification of the capacity of URM walls to this type of forces is required. The models in design codes are often conservative and do not capture the uncertainties required for estimating the failure probability of URM walls. This paper develops probabilistic capacity models for URM walls with hollow clay units subject to horizontal in-plane forces. The models are developed considering diagonal cracking, flexural/rocking, and sliding failure as possible failure modes. The models are constructed starting from existing physics-based models that attempt to capture the underlying physics, and then developing correction terms that improve the accuracy of the models and remove the inherent bias. Unknown parameters for the proposed models are calibrated using a Bayesian updating approach. The proposed models are probabilistic and capture the relevant uncertainties. The proposed models are used to assess fragility functions of example URM walls subject to horizontal in-plane forces. The comparison of the fragility functions shows the effect of selected variables.

Author keywords: Hollow clay units; Unreinforced masonry (URM) walls; In-plane forces; Bayesian approach; Probabilistic models; Fragility function.

Introduction

Unreinforced masonry (URM) is one of the most common and historically relevant construction methods. In URM buildings, the vertical load is carried by URM walls constructed from individual units, typically bound together by mortar. The same URM walls are also delegated to resist horizontal forces due, for example, to seismic events (Abrams 2001; Lourenço 2002). However, URM walls are particularly vulnerable to horizontal forces due to the low tensile strength of the mortar holding the units together. Past seismic events have shown this vulnerability [e.g., FEMA P-273 (FEMA 1997); Andreini et al. 2014; Giresini and Sassu 2018; Sorrentino et al. 2019]. This is particularly concerning for regions with a large presence of URM buildings and high seismicity (e.g., southern Europe, Middle East).

The behavior of URM walls subject to horizontal forces, both in-plane and out-of-plane, has been extensively investigated in the past few decades (e.g., Abrams and Shah 1992; Morandi et al. 2018). Different deterministic models have been proposed to quantify the capacity of URM walls. Simpler models consider the walls as homogeneous structural elements characterized by a nonlinear response (e.g., Benedetti and Benzoni 1984; Tomaževič 1987; Mengi and McNiven 1989; Willis et al. 2010; Penna et al. 2014a, b). However, these models do not consider the hysteretic behavior in defining the capacity of URM walls. Specifically, they do not account for the postpeak response and the brittle behavior of the units [as highlighted by Ignatakis et al. (1989)], and the mortar interface between units [as highlighted by Page (1978) and Lourenço et al. (1994)]. Among others, Rots (1991), Gabor et al. (2006), and Grande et al. (2013) considered the hysteretic behavior using finite-element (FE) modeling. However, FE modeling can be computationally expensive and might not be viable for the design and assessment of existing URM buildings. In design codes, the modeling often reverts to simpler analytical formulations, where the walls are modeled as a homogeneous medium (e.g., Pietruszczak and Niu 1992; Anthoine 1995). These formulations for different modes of failure are obtained based on the results of both FE modeling and experimental results.

The level of detail in the design codes varies by region. The European Code (CEN 2004, 2005b) and the Italian Building Code (NTC 2018) contain some of the most detailed specifications and models for URM walls subject to horizontal forces. They consider diagonal cracking, flexure/rocking, and sliding as modes of failure. They use models from Turnsek and Čačovic (1970), Turnsek and

Ph.D. Student, Dept. of Civil and Environmental Engineering and MAE Center, Univ. of Illinois at Urbana-Champaign, Newmark Civil Engineering Laboratory, 205 North Mathews Ave., Urbana, IL 61801−2352. (corresponding author). ORCID: https://orcid.org/0000-0002-1946-3940. Email: leandro@illinois.edu

Staff Member, Occupational Health and Safety and Environmental Protection Unit, European Organization for Nuclear Research, Esplanade des Particules, 1, 1217 Meyrin, Switzerland. ORCID: https://orcid.org/0000-0001-8474-4397

Professor, Dept. of Civil and Environmental Engineering and Director, MAE Center, Univ. of Illinois at Urbana-Champaign, Newmark Civil Engineering Laboratory, 205 North Mathews Ave., Urbana, IL 61801−2352.

Professor, Dept. of Civil, Environmental Engineering and Architecture, Univ. of Cagliari, Via Marengo, 2, 09123 Cagliari, Italy.
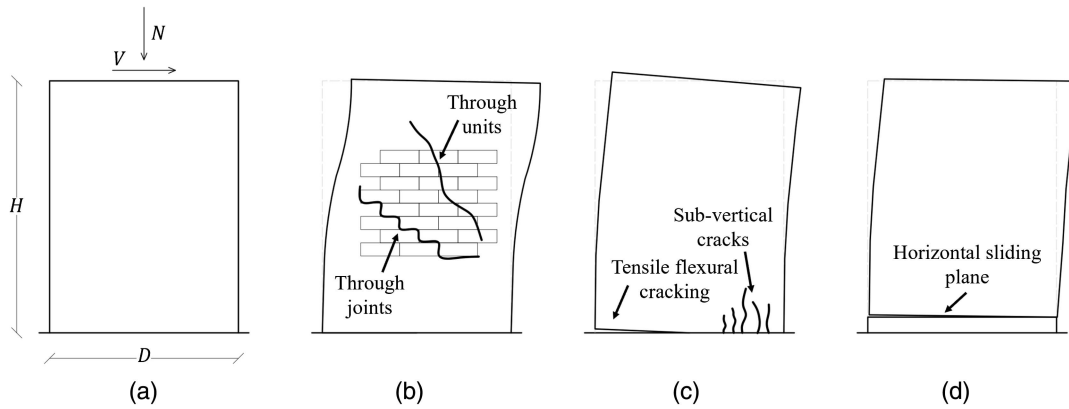
Fig. 1. (a) Dimensions and loads acting on the URM wall and diagram for the different failure modes; (b) diagonal cracking; (c) flexure/rocking; and (d) sliding failure.

Sheppard (1980), Hendry (1981), Abrams and Shah (1992), and Magenes and Calvi (1997) in an approach that accounts for the uncertainties related to the compressive and shear strengths. Such uncertainties are approximately incorporated by using preset values of partial safety factors. However, this approach does not account for other relevant uncertainties like model uncertainties (Gardoni et al. 2002; Murphy et al. 2011), and ultimately does not provide estimates of the actual failure probabilities. Annex D of the European Code EN 1990 (CEN 2005a) started to acknowledge reliability methods for statistical determination of resistance models. However, such methods are presented for general design purposes and have not been tailored to the field of URM. More recently, fragility estimates and probabilistic formulations for URM walls (e.g. Ruiz-Garcia and Negrete 2009) and buildings (e.g., Lagomarsino and Cattari 2014) have been developed. However, such formulations are purely empirical and the fragility functions are obtained by simple curve-fitting of the results of laboratory experiments and site surveys.

In this paper, we propose novel physics-based probabilistic models for the capacity of URM walls subject to horizontal, in-plane forces. This paper considers diagonal cracking, flexure/rocking, and sliding as modes of failure. The proposed trivariate models are formulated, following Gardoni et al. (2002), by adding model correction terms to existing physics-based models. The models selected for this paper can be found in the European Design Code (CEN 2005b) and in the Italian Building Code (NTC 2018). The addition of correction terms improves the accuracy and reduces the bias of the original models. The model correction terms include explanatory functions that are based on the physics of the phenomena and unknown model parameters that are calibrated using experimental data. We calibrate the unknown parameters using a Bayesian approach with a set of 108 experimental results on URM walls with different geometric and material characteristics. We formulate the likelihood function accounting for the contribution of both failure data and lower bound data, and we develop a trivariate model considering all possible failure modes at the same time, accounting for their correlation.

By adding correction terms to models currently available, the new formulations shed light on the limitations of the common practice. In addition, the proposed models account for the prevailing uncertainties (Gardoni et al. 2002; Murphy et al. 2011). We use the proposed models to obtain fragility functions for typical URM walls. By comparing the fragility functions of different walls, we can quantify the effect of selected variables on the wall capacity. As an example, we investigate the effect of the vertical load and slenderness ratio. While the paper focuses on single walls, the capacity

models and fragility functions can be used to assess the reliability of complete structures (e.g., URM buildings). The results highlighted in this work can be used as a starting point for discussing the variables that play a role in the failure of URM walls subject to horizontal actions, and suggesting a possible revision of the existing models.

This paper is organized as follows. The next section describes the three considered failure modes and reviews the corresponding existing physics-based capacity models. Then, we present the formulation of the proposed models. Next, we introduce the experimental data and calibrate the models. Finally, we present the fragility functions of the typical URM wall and investigate the effect of selected variables.

Existing Physics-Based Capacity Models for URM Walls

This section summarizes the different failure modes for URM walls and the corresponding capacity models. The URM walls considered in this paper are subject to a vertical force N and a horizontal in-place force V, as shown in Fig. 1(a). The height of the walls is H and the width is D.

Diagonal Cracking Failure Mode

The failure is due to diagonal cracks that can either pass through the units or through the mortar joints (e.g., Morandi et al. 2018). Fig. 1(b) shows both paths in the same wall. However, typically only one of the two paths is experienced by a wall depending on the relative resistance of the units and mortar. Because the cracking through the units is more frequent, in the remainder of this paper, we only consider this path. The cracking through mortar joints is sometimes categorized as diagonal sliding or gaping (Marques and Lourenço 2011; Morandi et al. 2018), and more closely follows the physical behavior described in the section for sliding failure. Diagonal cracking usually occurs for high values of vertical loads acting on the wall, which is a common trait of URM walls of lower stories of buildings (Tomaževič 2009).

In this paper, we select the formula proposed by Turnsek and Čačovic (1970) for the diagonal cracking capacity $\hat{V}_d$, which is also adopted by the Italian Code (NTC 2018). This formula considers the wall as an isotropic linearly elastic element that becomes unable to carry the load when the principal tensile stress σ_I at the center of the wall attains a specified maximum (strength) value. Accordingly, $\hat{V}_d$ can be written as (NTC 2018)

$$\hat{V}_d = \frac{f_t D t}{b} \sqrt{1 + \frac{N}{f_t D t}} \qquad (1)$$

where f_t = tensile strength of URM; t = thickness of the wall; and $b = H/D$ (the slenderness ratio of the wall) for $1 \leq H/D < 1.5$, $b = 1$ for $H/D < 1$, and $b = 1.5$ for $H/D \geq 1.5$. The diagonal cracking highly depends on the heterogeneity of the wall. Factors that play a role include the properties of the components (mortar and units), the bonding strength between these components, and the bond pattern. The combined effect of these variables is generally hard to model, such that existing models tend to be overly conservative.

Flexure/Rocking Failure Mode

Flexure/rocking failure [schematically shown in Fig. 1(c)] usually starts with the cracking of the bed joints (i.e., the horizontal joints) on the side of the wall in tension (e.g., Morandi et al. 2018). The cracking causes a reduction in the section of the wall resisting vertical forces, which eventually leads to the failure in the portion of the wall in compression with the creation of subvertical cracks. Flexure/rocking is typical of slender URM walls subject to low and intermediate levels of vertical loads. For large vertical loads, the creation of diagonal cracking would be more likely as discussed earlier.

In modeling the flexure/rocking capacity, $\hat{V}_f$, the tensile strength of the URM wall is generally disregarded and the distribution of the compressive stresses on the toe is approximated with a constant rectangular distribution (stress block). Accordingly, $\hat{V}_f$ can be written as (NTC 2018)

$$\hat{V}_f = \frac{D}{\psi' H} \frac{N}{2} \left(1 - \frac{N}{0.85 f_c' D t}\right) \qquad (2)$$

where ψ' is a coefficient depending on the boundary conditions of the wall ($\psi' = 1$ for a fixed-free boundary condition, $\psi' = 0.5$ for a fixed-fixed boundary condition, and $\psi' = 0.75$ for intermediate boundary conditions); f_c' = compressive strength of the URM; and 0.85 is the coefficient used in the stress block approximation. The flexure/rocking mechanism for URM closely resembles the flexure mechanism for concrete beams, which has been extensively investigated in the literature. In addition, the heterogeneous nature of URM walls does not affect flexure/rocking to the same extent as diagonal cracking, and the homogeneous medium assumption is satisfactory in most cases. For these reasons, flexure/rocking can generally be modeled more easily than diagonal cracking.

Sliding Failure Mode

In sliding failure [schematically shown in Fig. 1(d)], a horizontal sliding plane is created, typically in one of the bed joints in the lower portion of the wall. Sliding failure usually occurs for low vertical loads such that the friction between rows of units provided by the mortar is also low. This is often the case in the top stories of buildings. Most literature describes the sliding failure capacity $\hat{V}_s$ using a Mohr-Coulomb failure type criterion, where the stress distribution on the lower part of the wall is approximated as linear (e.g., Magenes and Calvi 1997). According to Magenes and Calvi (1997) $\hat{V}_s$ can be written as

$$\hat{V}_s = \frac{1.5 f_{v0} D t + \mu N}{1 + 3 f_{v0} \frac{\psi' H t}{N}} \qquad (3)$$

where f_{v0} = shear strength of URM walls under no compressive stress; and μ = friction coefficient. Eq. (3) can be obtained from the formulation in the Italian code (NTC 2018) under the assumption of linear compressive stress distribution. The database used in this paper provides the value for μ for most of the specimens analyzed. If the value of μ is not provided, we assume $\mu = 0.4$, following the prescriptions of the Eurocode (CEN 2005a).

Formulation of Proposed Probabilistic Models

In this section, we propose probabilistic models starting from the existing physics-based models introduced in the previous section. The proposed models improve the accuracy of the existing models and account for the relevant uncertainties. Following Gardoni et al. (2002) and Tabandeh et al. (2020), we select the following form for the probabilistic predictive models for the capacity of the URM wall in the jth mode of failure (e.g., $j = d$ for diagonal cracking, f for flexure/rocking, and s for sliding):

$$Y_j(\mathbf{x}, \boldsymbol{\Theta}_j) = \hat{y}_j(\mathbf{x}) + \gamma_j(\mathbf{x}, \boldsymbol{\theta}_j) + \sigma_j \varepsilon_j \qquad (4)$$

where $Y_j(\mathbf{x}, \boldsymbol{\Theta}_j)$ = dimensionless capacity of the variable of interest or a suitable transformation {e.g., $\ln[V_j(\mathbf{x}, \boldsymbol{\Theta}_j)]$ where V_j = capacity in the jth mode of failure}; $\mathbf{x}$ = set of measurable variables (e.g., material properties and specimen dimensions) also called state variables; $\boldsymbol{\Theta}_j = (\boldsymbol{\theta}_j, \sigma_j)$ = vector of unknown parameters; $\hat{y}_j(\mathbf{x})$ = existing physics-based model (e.g., one of the models described in the previous section) or a suitable transformation {e.g., $\ln[\hat{V}_j(\mathbf{x})]$}; $\gamma_j(\mathbf{x}, \boldsymbol{\theta}_j)$ = correction term; and $\sigma_j \varepsilon_j$ = model error, where ε_j = random variable with zero mean and unit variance, and σ_j = standard deviation of the model error. For given $\mathbf{x}$ and $\boldsymbol{\theta}_j$, the variance of the model is σ_j^2. The model formulation makes three assumptions: (1) the additivity of $\sigma_j \varepsilon_j$ (additivity assumption); (2) that ε_j has a normal distribution (normality assumption); and (3) that σ_j^2 is independent of $\mathbf{x}$ (homoskedasticity). We can at least approximately satisfy these assumptions with a suitable transformation (e.g., the natural logarithm) of the quantity of interest (Box and Cox 1964).

Following Gardoni et al. (2002), the term $\gamma_j(\mathbf{x}, \boldsymbol{\theta}_j)$ can be written as a linear combination of a set of p_j explanatory dimensionless functions $h_i(\mathbf{x})(i = 1, \ldots, p_j)$

$$\gamma_j(\mathbf{x}, \boldsymbol{\theta}_j) = \boldsymbol{\theta}_j \boldsymbol{h}_j(\mathbf{x}) = \sum_{i=1}^{p_j} \theta_{ji} h_{ji}(\mathbf{x}) \qquad (5)$$
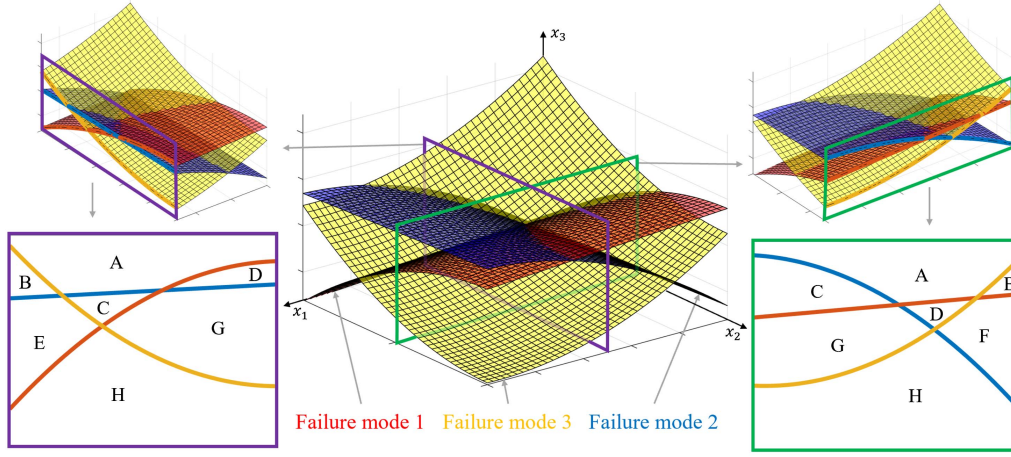
where $\boldsymbol{\theta}_j = [\theta_{j1}, \ldots, \theta_{jp_j}]$ is the vector of unknown parameters; and $\boldsymbol{h}_j(\mathbf{x}) = [\boldsymbol{h}_{j1}(\mathbf{x}), \ldots, \boldsymbol{h}_{jp_j}(\mathbf{x})]$ is the vector of explanatory functions. Because $\hat{y}_j(\mathbf{x})$ is physics-based and $\boldsymbol{h}_j(\mathbf{x})$ is also constructed based on physical/mechanical considerations, the probabilistic model $Y_j(\mathbf{x}, \boldsymbol{\Theta}_j)$ is also physics-based.

Bayesian Parameter Estimation

We use a Bayesian updating to obtain estimates for the values of $\boldsymbol{\Theta}_j$. We obtain the posterior probability density function (PDF) of $\boldsymbol{\Theta}_j$, $f(\boldsymbol{\Theta}_j)$, using the following formula:

$$f(\boldsymbol{\Theta}_j) = \kappa L(\boldsymbol{\Theta}_j) p(\boldsymbol{\Theta}_j) \qquad (6)$$

where $\kappa = [\int L(\boldsymbol{\Theta}_j) p(\boldsymbol{\Theta}_j) d\boldsymbol{\Theta}_j]^{-1}$ is a normalizing factor, necessary for the integral of the posterior distribution over the whole support to be equal to 1; $L(\boldsymbol{\Theta}_j)$ is the likelihood function, representing the information that can be inferred from the experimental observations; and $p(\boldsymbol{\Theta}_j)$ is the prior distribution, incorporating the knowledge about $\boldsymbol{\Theta}_j$ before the collection of data.

Fig. 2. Representation of data types for a bivariate model.

A: Failure in all modes
B: Failure in mode 1 and 2   E: Failure in mode 1 only
C: Failure in mode 1 and 3   F: Failure in mode 2 only
D: Failure in mode 2 and 3   G: Failure in mode 3 only
H: No failure

Likelihood Function and Prior Distribution for a Univariate Model

The likelihood function is proportional to the probability of observing the experimental outcome for given values of $\boldsymbol{\Theta}_j$. According to Gardoni et al. (2002), three different types of outcomes are possible when testing the kth specimen for the jth mode of failure. Each type provides different information about the quantity $r_{jk}(\boldsymbol{\theta}_j)$, defined as

$$r_{jk}(\boldsymbol{\theta}_j) = Y_{jk} - \hat{y}_j(\mathbf{x}) - \gamma_j(\mathbf{x}, \boldsymbol{\theta}_j) \tag{7}$$

where Y_{jk} is the recorded value of the variable of interest (or a suitable transformation) for the kth specimen. If Y_{jk} is recorded at the instant of failure then we have a failure datum, such that $Y_{jk} = \hat{y}_j(\mathbf{x}) + \gamma_j(\mathbf{x}, \boldsymbol{\theta}_j) + \sigma_j\varepsilon_{jk}$ or $\sigma_j\varepsilon_{jk} = r_{jk}(\boldsymbol{\theta}_j)$, where ε_{jk} denotes the outcome of the model error term. If the specimen does not fail or fails in a different mode of failure, then Y_{jk} is a lower bound censored datum, such that $Y_{jk} > \hat{y}_j(\mathbf{x}) + \gamma_j(\mathbf{x}, \boldsymbol{\theta}_j) + \sigma_j\varepsilon_{jk}$ or $\sigma_j\varepsilon_{jk} > r_{jk}(\boldsymbol{\theta}_j)$. Finally, if the specimen fails before reaching Y_{jk}, then Y_{jk} is an upper bound censored datum, and $Y_{jk} < \hat{y}_j(\mathbf{x}) + \gamma_j(\mathbf{x}, \boldsymbol{\theta}_j) + \sigma_j\varepsilon_{jk}$ or $\sigma_j\varepsilon_{jk} < r_{jk}(\boldsymbol{\theta}_j)$. Considering the different outcomes as statistically independent, we can express the likelihood as

$$L(\boldsymbol{\Theta}_j) \propto \underbrace{\prod P[\sigma_j\varepsilon_{jk} = r_{jk}(\boldsymbol{\theta}_j)]}_{\text{Failure data}}$$
$$\times \underbrace{\prod P[\sigma_j\varepsilon_{jk} > r_{jk}(\boldsymbol{\theta}_j)]}_{\text{Lower bound data}}$$
$$\times \underbrace{\prod P[\sigma_j\varepsilon_{jk} < r_{jk}(\boldsymbol{\theta}_j)]}_{\text{Upper bound data}} \tag{8}$$

Assuming that the errors are normally distributed (normality assumption) we can rewrite Eq. (8) as

$$L(\boldsymbol{\Theta}_j) \propto \underbrace{\prod \frac{1}{\sigma_j}\varphi\left[\frac{r_{jk}(\boldsymbol{\theta}_j)}{\sigma_j}\right]}_{\text{Failure data}} \times \underbrace{\prod \Phi\left[-\frac{r_{jk}(\boldsymbol{\theta}_j)}{\sigma_j}\right]}_{\text{Lower bound data}}$$
$$\times \underbrace{\prod \Phi\left[\frac{r_{jk}(\boldsymbol{\theta}_j)}{\sigma_j}\right]}_{\text{Upper bound data}} \tag{9}$$

where $\varphi(\cdot)$ and $\Phi(\cdot)$ denote the standard normal PDF and standard normal cumulative distribution function (CDF).

The prior distribution should incorporate the knowledge available before the experiments are performed. When no such knowledge is available, a noninformative prior should be used. In this paper, we choose the noninformative prior proposed by Box and Tiao (2011)

$$p(\boldsymbol{\Theta}_j) = p(\boldsymbol{\theta}_j, \sigma_j) \cong p(\sigma_j) = \frac{1}{\sigma_j} \tag{10}$$

We use Eqs. (8)–(10) to obtain the posterior statistics of $\boldsymbol{\Theta}_j$. We denote the posterior mean vector for $\boldsymbol{\Theta}_j$ and the posterior covariance matrix as $\mathbf{M}_{\boldsymbol{\Theta}_j}$ and $\boldsymbol{\Sigma}_{\boldsymbol{\Theta}_j\boldsymbol{\Theta}_j}$. The computation of these statistics requires a multifold integration over the Bayesian kernel $L(\boldsymbol{\Theta}_j)p(\boldsymbol{\Theta}_j)$. In this paper, we use the delayed rejection adaptive Markov chain Monte Carlo (Haario et al. 2006).

Likelihood Function and Prior Distribution for the Multivariate Model

To facilitate the understanding of the likelihood formulation for the multivariate case, let us consider a URM wall that has failed in diagonal cracking during a laboratory test. In this case, the value recorded during the test corresponds to the diagonal cracking capacity of the specimen, while both rocking and sliding capacity can be assumed to be larger than the recorded value. In other words, the recorded value can be registered as a failure datum for the diagonal cracking capacity and as a lower bound datum for the rocking capacity and sliding capacity. In general, for a q-variate model, data can be categorized into a total of 2^q combinations. Fig. 2 exemplifies this idea for a trivariate model. Thus, the classification introduced in the previous section (failure data, lower bound data, and upper bound data) applies unchanged to the multivariate case, but a single observation can fall into different categories for the different capacity measures.

Tables 1 and 2 show the formulas that can be used to compute the likelihood in case of a bivariate and a trivariate model, respectively (considering only failure data and lower bound data). We obtained these formulas under the assumptions that the error terms

Table 1. Probability terms for bivariate capacity model with lower bounds and failure data

	Capacity model 1	
Capacity model 2	Failure datum	Lower bound
Failure datum	$\dfrac{1}{\sigma_{1\|2}}\varphi\left[\dfrac{r_{1i}(\boldsymbol{\theta})-\mu_{1\|2}}{\sigma_{1\|2}}\right]\dfrac{1}{\sigma_2}\varphi\left[\dfrac{r_{2i}(\boldsymbol{\theta})}{\sigma_2}\right]$	$\Phi\left[-\dfrac{r_{1i}(\boldsymbol{\theta})-\mu_{1\|2}}{\sigma_{1\|2}}\right]\dfrac{1}{\sigma_2}\varphi\left[\dfrac{r_{2i}(\boldsymbol{\theta})}{\sigma_2}\right]$
Lower bound	$\Phi\left[-\dfrac{r_{2i}(\boldsymbol{\theta})-\mu_{2\|1}}{\sigma_{2\|1}}\right]\dfrac{1}{\sigma_1}\varphi\left[\dfrac{r_{1i}(\boldsymbol{\theta})}{\sigma_1}\right]$	$\int_{r_{2i}}^{\infty}\Phi\left[-\dfrac{r_{1i}(\boldsymbol{\theta})-\mu_{1\|\zeta}}{\sigma_{1\|2}}\right]\dfrac{1}{\sigma_2}\varphi\left[\dfrac{\zeta}{\sigma_2}\right]d\zeta$

Source: Data from Gardoni et al. (2002).

Note: $\mu_{k\|l}=\rho_{kl}(\sigma_k/\sigma_l)r_{li}$, $\sigma_{k\|l}=\sigma_k\sqrt{1-\rho_{kl}^2}k$, $l=1,2$ and $\mu_{1\|\zeta}=\rho_{12}(\sigma_1/\sigma_2)\zeta$.

Table 2. Probability terms for trivariate capacity model with lower bounds and failure data

Type of data	Probability terms
Failure data for all models	$\dfrac{1}{\sigma_{k\|lm}}\varphi\left[\dfrac{r_{ki}(\boldsymbol{\theta})-\mu_{k\|lm}}{\sigma_{k\|lm}}\right]\dfrac{1}{\sigma_{l\|m}}\varphi\left[\dfrac{r_{li}(\boldsymbol{\theta})-\mu_{l\|m}}{\sigma_{l\|m}}\right]\dfrac{1}{\sigma_m}\varphi\left[\dfrac{r_{mi}(\boldsymbol{\theta})}{\sigma_m}\right]$
Lower bound for model k Failure datum for model l, m	$\Phi\left[-\dfrac{r_{ki}(\boldsymbol{\theta})-\mu_{k\|lm}}{\sigma_{k\|lm}}\right]\dfrac{1}{\sigma_{l\|m}}\varphi\left[\dfrac{r_{li}(\boldsymbol{\theta})-\mu_{l\|m}}{\sigma_{l\|m}}\right]\dfrac{1}{\sigma_m}\varphi\left[\dfrac{r_{mi}(\boldsymbol{\theta})}{\sigma_m}\right]$
Lower bound for model k, l Failure datum for model m	$\left\{\int_{r_{li}}^{\infty}\Phi\left[-\dfrac{r_{ki}(\boldsymbol{\theta})-\mu_{k\|\zeta m}}{\sigma_{k\|lm}}\right]\dfrac{1}{\sigma_{l\|m}}\varphi\left[\dfrac{\zeta-\mu_{l\|}}{\sigma_{l\|m}}\right]d\zeta\right\}\dfrac{1}{\sigma_m}\varphi\left[\dfrac{r_{mi}(\boldsymbol{\theta})}{\sigma_m}\right]$
Lower bound for all models	$\int_{r_{mi}}^{\infty}\left\{\int_{r_{li}}^{\infty}\Phi\left[-\dfrac{r_{ki}(\boldsymbol{\theta})-\mu_{k\|\zeta\xi}}{\sigma_{k\|lm}}\right]\dfrac{1}{\sigma_{l\|m}}\varphi\left[\dfrac{\zeta-\mu_{l\|\xi}}{\sigma_{l\|m}}\right]d\zeta\right\}\dfrac{1}{\sigma_m}\varphi\left[\dfrac{\xi}{\sigma_m}\right]d\xi$

Note: $\mu_{k\|lm}=\frac{1}{1-\rho_{lm}^2}\left\{[\rho_{kl}+\rho_{km}\rho_{ml}]\frac{\sigma_k}{\sigma_l}r_{li}+[\rho_{km}+\rho_{kl}\rho_{lm}]\frac{\sigma_k}{\sigma_m}r_{mi}\right\}$ $k,l,m=1,2,3$ $k\neq l\neq m$; $\mu_{k\|\zeta m}=\frac{1}{1-\rho_{lm}^2}\left\{[\rho_{kl}+\rho_{km}\rho_{ml}]\frac{\sigma_k}{\sigma_l}\zeta+[\rho_{km}+\rho_{kl}\rho_{lm}]\frac{\sigma_k}{\sigma_m}r_{mi}\right\}$ $k,l,m=1,2,3$ $k\neq l\neq m$; $\mu_{k\|\zeta\xi}=\frac{1}{1-\rho_{lm}^2}\left\{[\rho_{kl}+\rho_{km}\rho_{ml}]\frac{\sigma_k}{\sigma_l}\zeta+[\rho_{km}+\rho_{kl}\rho_{lm}]\frac{\sigma_k}{\sigma_m}\xi\right\}$ $k,l,m=1,2,3$ $k\neq l\neq m$; $\mu_{k\|l}=\rho_{kl}\frac{\sigma_k}{\sigma_l}r_{li}$ $k,l=1,2$ $k\neq l$; $\sigma_{k\|lm}=\sigma_k\sqrt{1+\frac{1}{1-\rho_{lm}^2}[\rho_{kl}(\rho_{km}\rho_{ml}-\rho_{kl})+\rho_{km}(\rho_{kl}\rho_{lm}-\rho_{km})]}$ $k,l,m=1,2,3$ $k\neq l\neq m$;. $\sigma_{k\|l}=\sigma_k\sqrt{1-\rho_{kl}^2}$ $k,l=1,2$ $k\neq l$.

ε_{jk} can be modeled with a multinormal PDF with given covariance matrix $\boldsymbol{\Sigma}$.

We use the following noninformative prior to reflect the lack of knowledge before the collection of data (Gardoni et al. 2002):

$$p(\boldsymbol{\theta},\boldsymbol{\Sigma})\cong p(\boldsymbol{\Sigma})=|\boldsymbol{\Sigma}|^{-\frac{q+1}{2}} \tag{11}$$

where $\boldsymbol{\theta}=[\boldsymbol{\theta}_d,\boldsymbol{\theta}_f,\boldsymbol{\theta}_s]=[\theta_{ji}]$.

Stepwise Deletion

Ideally, models need to be as parsimonious as possible (e.g., simple and accurate). A simple model is characterized by a small number of parameters p_j. An accurate model is characterized by a small value of standard deviation σ_j. Typically, reducing p_j tends to increase σ_j. To find a compromise, we can use a stepwise deletion. A traditional stepwise deletion based on p-values (Stone 1996) is not applicable when there are censored data. In this paper, we use the procedure in Gardoni et al. (2002), which is applicable also to the case of censored data. The procedure starts with all the candidate explanatory functions, and at each step removes the least important explanatory function based on the coefficient of variation (COV) of the corresponding θ_{ji}. The model is then reassessed with the reduced number of parameters. The procedure continues until σ_j grows to an undesirable value or there is an undesirable increase in σ_j with respect to reduction in model complexity.

Proposed Physics-Based Probabilistic Capacity Models for URM Walls

In this section, we develop physics-based probabilistic capacity models for URM walls. We calibrate the proposed models using test results on unconfined URM specimens with hollow clay units subject to in-plane loads. The specimens are obtained from Frumento et al. (2009) and Morandi et al. (2018). Repetitions in the two databases were properly identified so that each specimen was only counted once. Confined masonry specimens were excluded from the analysis. The total number of specimens is 108. All the specimens were subject to cyclic lateral horizontal in-plane forces under a constant vertical load. The horizontal load was applied in the form of a controlled displacement. The amplitude of the displacement was gradually increased up to the collapse of the specimens. Table 3 summarizes the occurrences of each mode of failure. The off-diagonal terms represent mixed modes of failures.

Table 3. Occurrences of each mode of failure

Mode of failure	Diagonal cracking	Flexure/rocking	Sliding
Diagonal cracking	56	—	—
Flexure/rocking	10	36	—
Sliding	1	2	3

Because of the high vertical load in the test environment, the sliding mode of failure only occurred for six specimens.

A logarithmic transformation of both $V_j(\mathbf{x}, \boldsymbol{\Theta}_j)$ and $\hat{V}_j(\mathbf{x})$ is applied to approximately satisfy the additivity, normality, and homoskedasticity assumptions. So, Eq. (4) is written as

$$\ln[V_j(\mathbf{x}, \boldsymbol{\Theta}_j)] = \ln[\hat{V}_j(\mathbf{x})] + \gamma_j(x, \boldsymbol{\theta}_j) + \sigma_j \varepsilon_j \quad j = d, f, s \quad (12)$$

Ideally, both $V_j(\mathbf{x}, \boldsymbol{\Theta}_j)$ and $\hat{V}_j(\mathbf{x})$ should be dimensionless quantities. However, the logarithmic transformation allows us to rewrite Eq. (12) as

$$\ln\left[\frac{V_j(\mathbf{x}, \boldsymbol{\Theta}_j)}{\hat{V}_j(\mathbf{x})}\right] = \gamma_j(x, \boldsymbol{\theta}_j) + \sigma_j \varepsilon_j \quad j = d, f, s \quad (13)$$

which can be used even if $V_j(\mathbf{x}, \boldsymbol{\Theta}_j)$ and $\hat{V}_j(\mathbf{x})$ are not dimensionless. Based on the normality assumption, the 67% confidence interval for the transformed value of the capacity can be written as

$$\{\ln[\hat{V}_j(\mathbf{x})] + \gamma_j(\mathbf{x}, \boldsymbol{\theta}_j) - \sigma_j, \ln[\hat{V}_j(\mathbf{x})] + \gamma_j(\mathbf{x}, \boldsymbol{\theta}_j) + \sigma_j\} \quad (14)$$

which corresponds to the following interval for the untransformed value of the capacity:

$$\{\hat{V}_j(\mathbf{x})e^{\gamma_j(\mathbf{x}, \boldsymbol{\theta}_j)}e^{-\sigma_j}, \hat{V}_j(\mathbf{x})e^{\gamma_j(\mathbf{x}, \boldsymbol{\theta}_j)}e^{\sigma_j}\} \quad (15)$$

Model Correction

We select the same set of explanatory functions for the three failure modes. To capture the presence of a possible constant bias in $\ln[\hat{V}_j(\mathbf{x})]$, we select $h_1(\mathbf{x}) = 1$. To assess the possible effects of the void percentage (percentage of all holes) in the units, we select $h_2(\mathbf{x}) = Vol_{\text{voids}}/Vol_{\text{tot}}$, where Vol_{voids} is the volume of the voids and Vol_{tot} is the gross volume of the unit. To assess the influence of the geometric dimensions of the units, we select $h_3(\mathbf{x}) = h/d$, where h and d are the height and the width of the unit, respectively. To detect any potential influence of the number of rows of units on the capacity of the URM wall, we select $h_4(\mathbf{x}) = h/H$, where H is the total height of the wall. Because $\hat{V}_j$ does not include any variable related to the units, the explanatory functions $h_2(\mathbf{x})$, $h_3(\mathbf{x})$, and $h_4(\mathbf{x})$ explore the possible effects of such variables. To detect any possible underestimation or overestimation of the contribution of the slenderness ratios of the wall in both directions, we select $h_5(\mathbf{x}) = t/H$ and $h_6(\mathbf{x}) = H/D$. To capture the effect of the tensile strength of the units f_t and of the compressive strength of the mortar f_{cM}, we select $h_7(\mathbf{x}) = f_t/f_c'$ and $h_8(\mathbf{x}) = f_{cM}/f_c'$ (where the compressive strength of the URM f_c' is used to obtain dimensionless explanatory variables). To capture the effect of the vertical load on the wall N as a fraction of the total vertical load N_{max} that the wall can sustain, we select $h_9(\mathbf{x}) = N/N_{\text{max}}$ (where N_{max} is provided along with the data). To capture the effect of the thickness of the bed-joints, we select the categorical explanatory function $h_{10}(\mathbf{x})$ equal to 0 for general purpose mortar and 1 for thin layer mortar. To capture the effect of the head-joint type, we select the categorical explanatory function $h_{11}(\mathbf{x})$ equal to −1 for filled joints, −0.5 for thin-filled joints, 0 for mortar pocket joints, 0.5 for unfilled joints, and 1 for tongue-and-groove joints. Finally, to capture the effect of the boundary conditions, we select the categorical explanatory function $h_{12}(\mathbf{x}) = \psi'$, with ψ' as defined earlier as in input to Eq. (2). Table 4 reports the range of variation of the selected explanatory functions for the 108 specimens.

Table 4. Ranges of the selected explanatory functions for the specimens

Explanatory function	Range
$h_1(\mathbf{x})$	1.00
$h_2(\mathbf{x})$	[0.41, 0.54]
$h_3(\mathbf{x})$	[0.48, 1.03]
$h_4(\mathbf{x})$	[0.07, 0.20]
$h_5(\mathbf{x})$	[0.06, 0.26]
$h_6(\mathbf{x})$	[0.67, 2.5]
$h_7(\mathbf{x})$	[0.01, 0.08]
$h_8(\mathbf{x})$	[0.43, 3.43]
$h_9(\mathbf{x})$	[0.02, 0.29]
$h_{10}(\mathbf{x})$	[0.00, 1.00]
$h_{11}(\mathbf{x})$	[−1.00, 1.00]
$h_{12}(\mathbf{x})$	[0.50, 1.00]
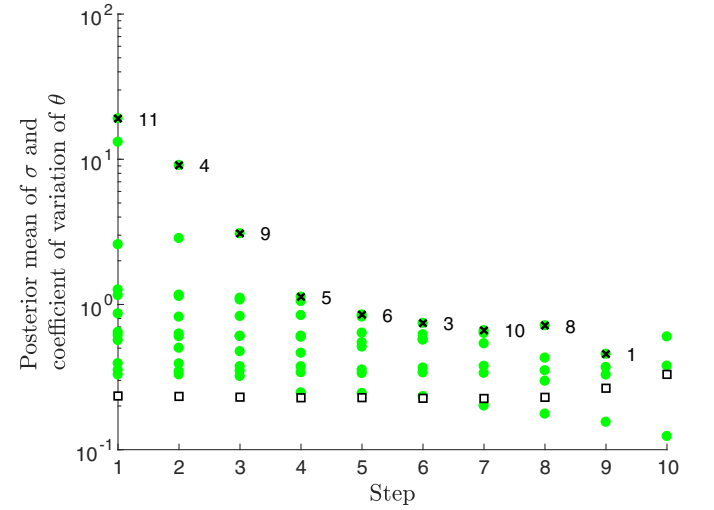
Fig. 3. Stepwise deletion process for the diagonal cracking capacity model.

Bayesian Parameter Estimation and Stepwise Deletion

This section provides the results for the univariate models and the trivariate model.

Univariate Model for Diagonal Cracking
Fig. 3 shows the results of the stepwise deletion process. At each step, the dots represent the values for the coefficients of variation of the different θ_{di}'s, while the square represents the value for the posterior mean of σ_d.

At the first step, the parameter with the largest coefficient of variation is θ_{d11} (COV = 19.02). The coefficient of variation of θ_{d11} is much larger than the coefficients of variation of the other terms and the standard deviation of the model ($\sigma_d = 0.215$). For this reason, we decided to drop this term; this is graphically represented in the figure with a cross over the dot representing the coefficient of variation of the term that was dropped. Following the removal of the first term, we observed a 1% increase in σ_d, which we deemed acceptable. We repeated the same process until Step 9. After removing h_1, σ_d increased by 23%. This increase is deemed undesirable, therefore we kept h_1 in the model and stopped the deletion process. The reduced $\gamma_d(\mathbf{x}, \boldsymbol{\theta}_d)$ has the following final form:

$$\gamma_d(\mathbf{x}, \boldsymbol{\theta}_d) = \theta_{d1} + \theta_{d2}\frac{Vol_{\text{voids}}}{Vol_{\text{tot}}} + \theta_{d7}\frac{f_t}{f_c'} + \theta_{d12}\psi' \qquad (16)$$

Table 5 gives the posterior statistics of the five model parameters.
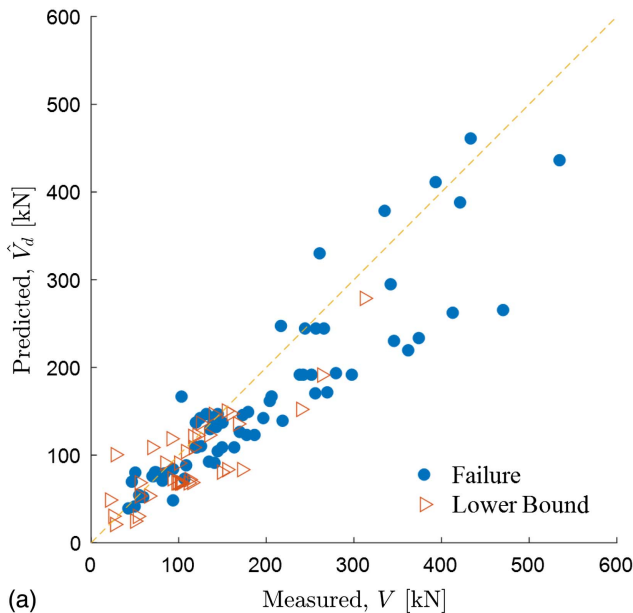
The following observations can be made based on the results of the stepwise deletion process and the parameter estimation:

- The h_1 is retained in the final model. This is an indication that $\hat{V}_d(\mathbf{x})$ has a systematic bias independent of $\mathbf{x}$.
- The $h_2(\mathbf{x})$ is also retained in the final model. This suggests that the properties of the units, neglected in most of the design codes (including $\hat{V}_d$), play an important role in the total capacity of the walls.
- The $h_7(\mathbf{x})$ and $h_{12}(\mathbf{x})$ are retained in the final model. These parameters are also included in $\hat{V}_d(\mathbf{x})$. By looking at the values of the θ_{di}'s associated with these explanatory functions, we can tell that $\hat{V}_d(\mathbf{x})$ overestimates ($\theta_{d7} < 0$) the effect of f_t (URM tensile strength) and it underestimates ($\theta_{d12} > 0$) the effect of ψ' (boundary conditions).

Fig. 4(a) shows the predicted versus measured capacity for each experiment. Ideally, the predicted capacity should be equal to the measured capacity if the sample fails in diagonal cracking (i.e., we have a failure datum). If the sample fails in a different mode (i.e., we have a lower bound datum), the predicted capacity for diagonal cracking should be greater than the measured capacity. So for a perfect model, failure data lie on the 1:1 line, and the lower bound data lie above it.

We can observe from Fig. 4(a) how the predicted capacity is generally lower than the measured one. This reflects the fact that the model proposed by the code tends to give conservative results. Fig. 4(b) shows the improvement in the prediction of the diagonal cracking capacity. The figure shows the median prediction based on the posterior statistics of $\boldsymbol{\theta}_d$ and $\varepsilon_d = 0$. The figure also shows the region within one standard deviation of the median value. The proposed model corrects the bias in the existing model and provides more accurate predictions. The failure data points are now closer to the 1:1 line and most of the lower bound data points lie above it.

Univariate Model for Flexure/Rocking

Fig. 5 shows the results of the stepwise deletion process for the flexure/rocking univariate model.

We carried out the deletion process for 10 steps until the removal of h_3 caused a 9.3% increase in σ_f, which is deemed undesirable. Therefore, we kept h_3 in the model and stopped the deletion process. The final form of the bias correction term is
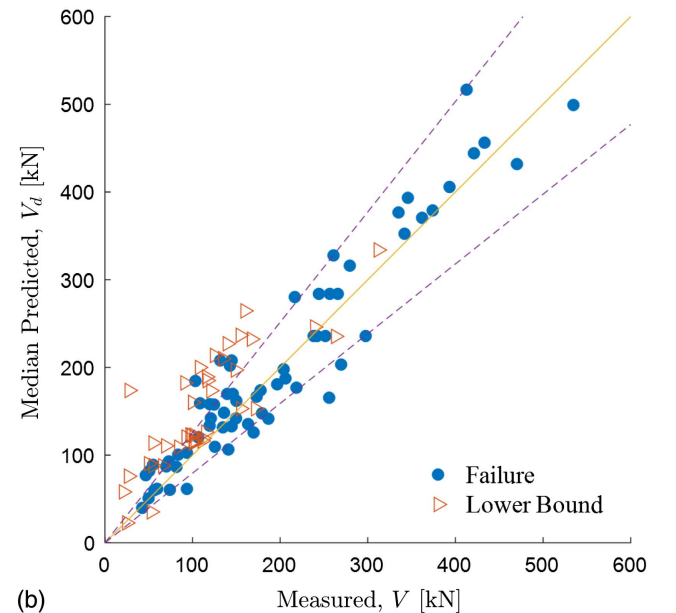
$$\gamma_f(\mathbf{x}, \boldsymbol{\theta}_f) = \theta_{f2}\frac{Vol_{\text{voids}}}{Vol_{\text{tot}}} + \theta_{f3}\frac{h}{d} + \theta_{f7}\frac{f_t}{f_c'} \qquad (17)$$

Table 6 gives the posterior statistics of the three remaining θ_{fi} and σ_f.

We can make the following observations:

- The h_1 is not kept in the model, highlighting the lack of a constant bias.
- The h_2 and h_3 are kept in the model. These variables are related to the properties of the units, and are neglected in most of the codes (including $\hat{V}_f$).
- The h_7 is kept in the model. This suggests that, while it is generally not considered in design codes for this mode of failure, f_t (tensile strength of the URM) plays an important role in the value of the flexure/rocking capacity.

Fig. 6(a) shows the predicted versus measured capacity. The same comments provided for Fig. 4(a) also apply to this case. The addition of $\gamma_f(\mathbf{x}, \boldsymbol{\theta}_f)$ improves the accuracy of the model in particular for the lower bound data. The median predictions are shown in Fig. 6(b).

Table 5. Posterior statistics for Θ_d

Parameter	Mean	Standard deviation	Correlation coefficients				
			θ_{d1}	θ_{d2}	θ_{d7}	θ_{d12}	σ_d
θ_{d1}	0.520	0.235	1	—	—	—	—
θ_{d2}	−1.365	0.505	−0.50	1	—	—	—
θ_{d7}	−7.096	2.335	−0.12	−0.10	1	—	—
θ_{d12}	0.826	0.127	−0.17	−0.19	0.10	1	—
σ_d	0.230	0.021	0.05	−0.11	0.02	0.24	1

Fig. 4. Predicted capacity versus measured capacity for diagonal cracking: (a) existing model; and (b) probabilistic model.
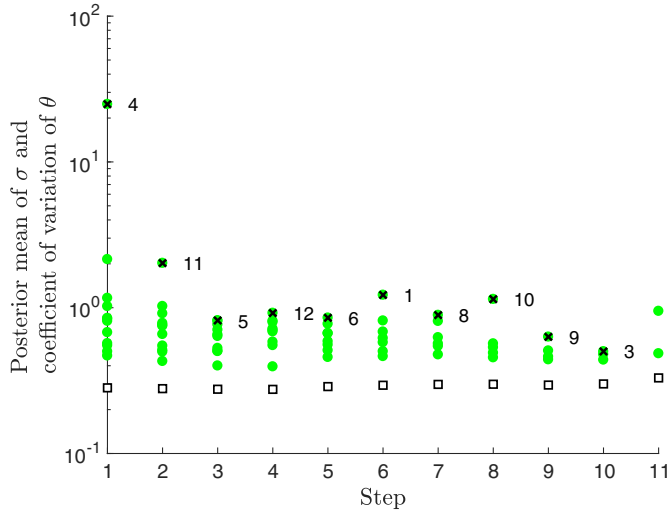
Fig. 5. Stepwise deletion process for the flexure/rocking capacity model.

Table 6. Posterior statistics for Θ_f

| Parameter | Mean | Standard deviation | Correlation coefficients | | | |
			θ_{f2}	θ_{f3}	θ_{f7}	σ_f
θ_{f2}	−1.018	0.443	1	—	—	—
θ_{f3}	0.463	0.229	−0.52	1	—	—
θ_{f7}	6.441	3.072	−0.32	0.02	1	—
σ_f	0.293	0.030	0.11	−0.08	0.07	1

Univariate Model for Sliding

For the parameter estimation of the sliding model, there is an identifiability problem (Stone 1996) when we use all 12 explanatory functions because we only have six failure data. Given the number of failure data, we can only estimate a model with three explanatory functions (i.e., the calibration does not converge when

more explanatory function are used). Hence, we consider all possible combinations of three h_i's and select the model that has the smallest σ_s. The final form the model correction term for the sliding mode of failure is

$$\gamma_s(\mathbf{x}, \boldsymbol{\theta}_s) = \theta_{s2} \frac{Vol_{\text{voids}}}{Vol_{\text{tot}}} + \theta_{s3} \frac{h}{d} + \theta_{s8} \frac{f_{cM}}{f'_c} \qquad (18)$$

Table 7 shows the posterior statistics of the $\boldsymbol{\Theta}_s$ in the selected model. The value of σ_s ($\sigma_s = 0.523$) is significantly higher than σ_d and σ_f, so we do not proceed with further deletions.

We can make the following observations:

- The h_1 is not kept in the model, highlighting the lack of a constant bias.
- The h_2 and h_3 are kept in the model. These variables are related to the properties of the units, and are neglected in most of the codes (including $\hat{V}_s$).
- The h_8 is kept in the model and $\theta_{s8} > 0$. This suggests that the contribution of the compressive strength of the mortar to the sliding capacity is underestimated in the original model.

Fig. 7(a) shows the measured versus predicted capacity for sliding. The same comments provided for Fig. 4(a) apply to this case. The results following the calibration of the model are plotted in Fig. 7(b).

Trivariate Model

We calibrate the trivariate model to obtain the correlation coefficients between the parameters in $\boldsymbol{\Theta}_d$, $\boldsymbol{\Theta}_f$, and $\boldsymbol{\Theta}_s$ and between the model errors of the different failure modes, required for reliability analysis. The vector of uncertain parameters for the trivariate model is $\boldsymbol{\Theta} = (\boldsymbol{\Theta}_d, \boldsymbol{\Theta}_f, \boldsymbol{\Theta}_s, \rho_{df}, \rho_{ds}, \rho_{fs})$, where $\boldsymbol{\Theta}_d$, $\boldsymbol{\Theta}_f$, and $\boldsymbol{\Theta}_s$ contain the same parameters as the corresponding univariate models, and ρ_{df}, ρ_{ds}, and ρ_{fs} are the correlations between the error terms of the different models. We obtain the following noninformative prior distribution for the trivariate case from Eq. (11) with $q = 3$:

$$p(\boldsymbol{\Theta}) = \frac{1 + 2\rho_{df}\rho_{ds}\rho_{fs} - \rho_{df}^2 - \rho_{ds}^2 - \rho_{fs}^2}{\sigma_d \sigma_f \sigma_s} \qquad (19)$$
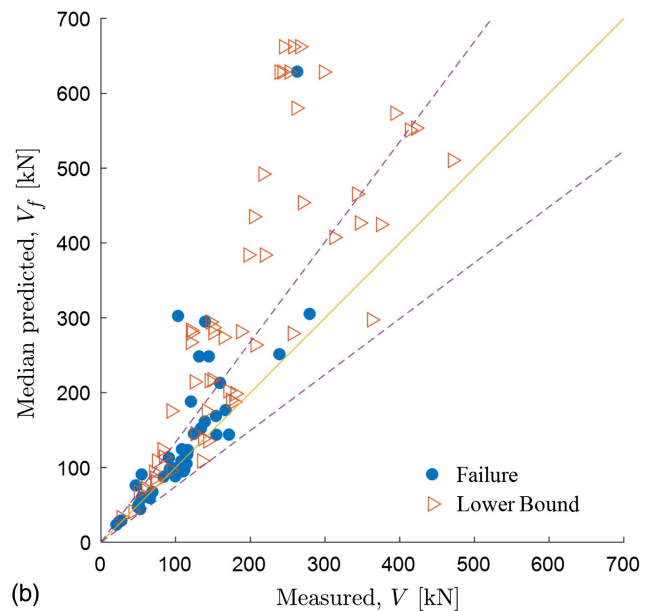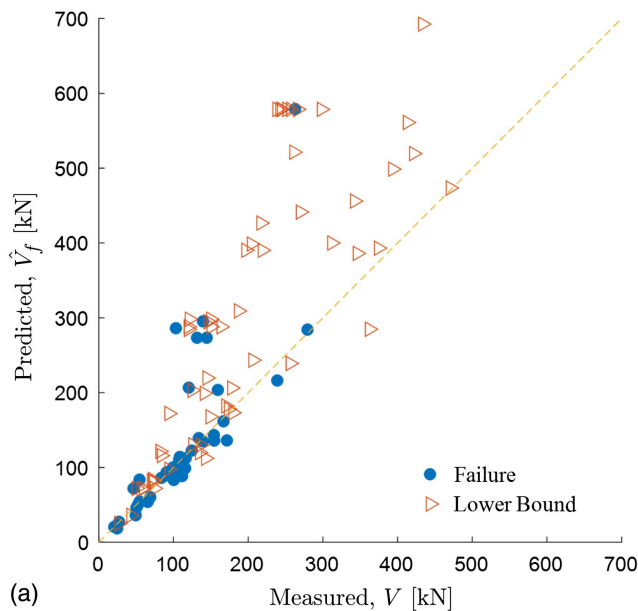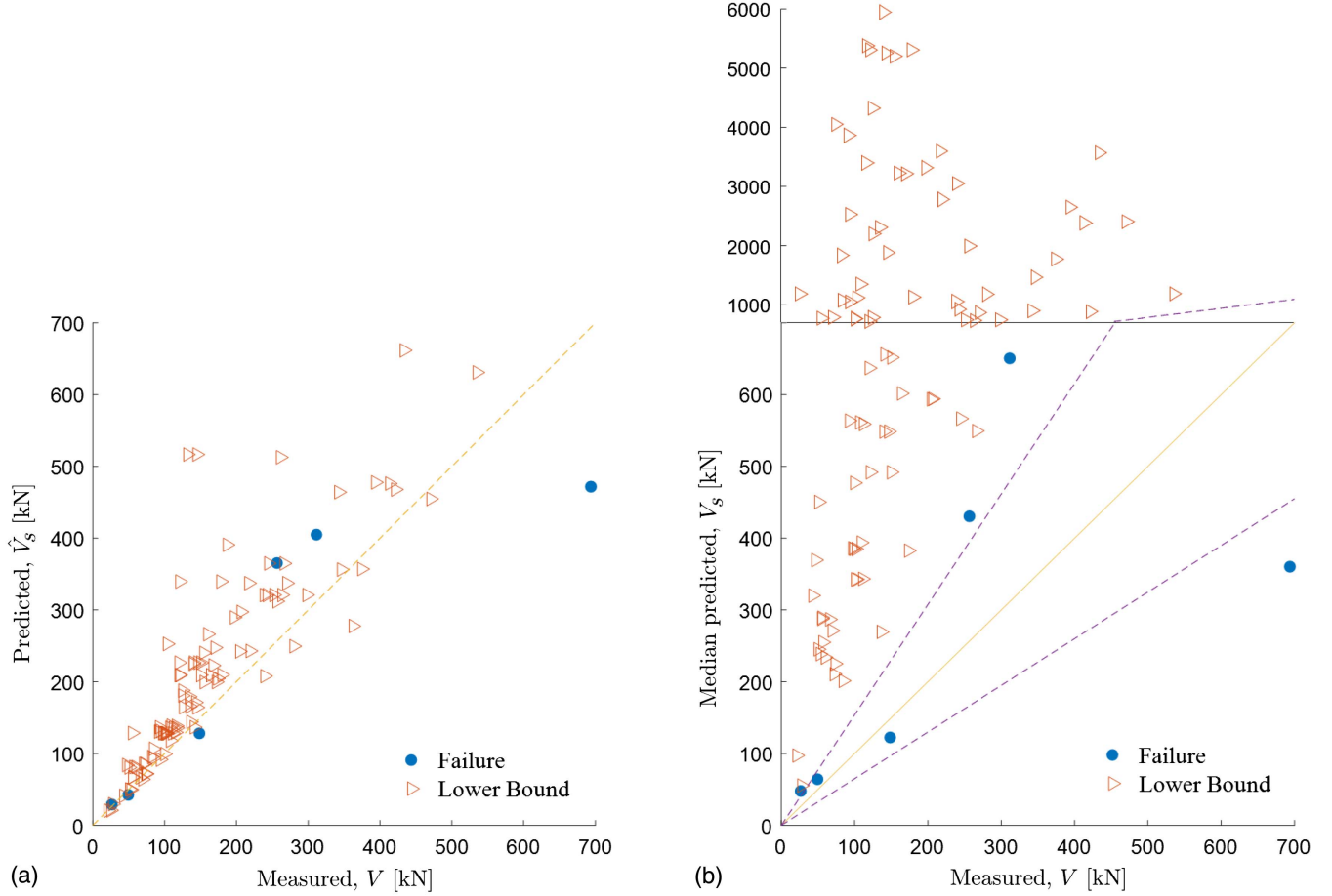

Fig. 6. Predicted capacity versus measured capacity for flexure/rocking: (a) existing model; and (b) probabilistic model.

Table 7. Posterior statistics for Θ_s

Parameter	Mean	Standard deviation	Correlation coefficients			
			θ_{s2}	θ_{s3}	Θ_{s8}	σ_s
θ_{s2}	2.007	2.449	1	—	—	—
θ_{s3}	−1.223	1.489	−0.40	1	—	—
θ_{s8}	1.322	1.217	0.26	−0.41	1	—
σ_s	0.523	0.358	0.34	−0.23	0.28	1

The results of the calibration are available in Table 8. As expected, the values of Θ_d, Θ_f, and Θ_s are the same as those obtained in the calibration of the univariate models (except for minor numerical differences). Therefore, the median predictions from the trivariate model for each mode are the same as the predictions from the univariate models. As a result, plots of the predicted versus measured capacity would be the same as in Figs. 4, 6, and 7.

Fig. 7. Predicted capacity versus measured capacity for sliding: (a) existing model; and (b) probabilistic model.

Table 8. Posterior statistics for Θ of the trivariate model

Parameter	Mean	Standard deviation	θ_{d1}	θ_{d2}	θ_{d7}	θ_{d12}	σ_d	θ_{f2}	θ_{f3}	θ_{f7}	σ_f	θ_{s2}	θ_{s3}	θ_{s8}	σ_s	ρ_{df}	ρ_{ds}	ρ_{sf}
θ_{d1}	0.633	0.225	1	—	—	—	—	—	—	—	—	—	—	—	—	—	—	—
θ_{d2}	−1.521	0.485	−0.92	1	—	—	—	—	—	—	—	—	—	—	—	—	—	—
θ_{d7}	−7.384	1.854	−0.05	−0.16	1	—	—	—	—	—	—	—	—	—	—	—	—	—
θ_{d12}	0.750	0.119	−0.17	−0.15	0.1	1	—	—	—	—	—	—	—	—	—	—	—	—
σ_d	0.222	0.020	0.05	−0.09	0.08	0.25	1	—	—	—	—	—	—	—	—	—	—	—
θ_{f2}	−0.987	0.387	−0.01	0.05	−0.05	−0.11	−0.03	1	—	—	—	—	—	—	—	—	—	—
θ_{f3}	0.431	0.202	0.01	−0.02	−0.04	0.09	−0.02	−0.93	1	—	—	—	—	—	—	—	—	—
θ_{f7}	6.608	2.723	−0.06	−0.03	0.28	0.13	0.12	−0.26	−0.07	1	—	—	—	—	—	—	—	—
σ_f	0.285	0.029	−0.04	0.01	0.07	0.03	0.08	0.15	−0.17	0.19	1	—	—	—	—	—	—	—
θ_{s2}	1.883	1.302	0.13	−0.1	−0.06	−0.08	−0.07	−0.11	0.16	−0.17	−0.08	1	—	—	—	—	—	—
θ_{s3}	−1.423	1.047	−0.2	0.17	0.06	0.11	0.09	0.05	−0.11	0.21	0.07	−0.87	1	—	—	—	—	—
θ_{s8}	1.414	0.828	0.2	−0.17	−0.05	−0.12	−0.08	0.06	−0.01	−0.21	−0.06	0.74	−0.94	1	—	—	—	—
σ_s	0.485	0.198	0.1	−0.06	−0.05	−0.08	−0.01	0.07	−0.03	−0.17	−0.05	0.77	−0.65	0.68	1	—	—	—
ρ_{df}	0.404	0.108	0.184	−0.1	−0.06	−0.32	−0.05	0.08	−0.03	−0.18	0.03	0.14	−0.19	0.18	0.08	1	—	—
ρ_{ds}	−0.274	0.413	−0.3	0.27	0.09	0.13	0.11	−0.01	−0.05	0.22	0.05	−0.37	0.52	−0.5	−0.31	−0.25	1	—
ρ_{sf}	−0.521	0.324	0.05	−0.07	0.06	0.03	0.09	0.14	−0.19	0.16	0.12	−0.2	0.15	−0.13	−0.24	0.01	0.37	1

Table 9. Properties of the URM wall used for the computation of the fragility functions

Variable	Type	Mean	Coefficient of variation
H	Deterministic	1,500 mm	—
D	Deterministic	1,500 mm	—
t	Deterministic	300 mm	—
h	Deterministic	230 mm	—
d	Deterministic	150 mm	—
% holes	Deterministic	50%	—
f_c	Lognormal	5 MPa	0.1
f_{cM}	Lognormal	9 MPa	0.1
f_{v0}	Lognormal	0.25 MPa	0.1
N	Lognormal	400 kN	0.25

Proposed Physics-Based Fragility Functions

The fragility is defined as the conditional probability of attaining or exceeding a prescribed limit state for a given demand (Gardoni et al. 2002). Mathematically, we first introduce the limit state function g_j (Ditlevsen and Madsen 1996; Gardoni 2017) for the jth mode of failure as

$$g_j(\mathbf{x}, \mathbf{\Theta}_j) = \ln[V_j(\mathbf{x}, \mathbf{\Theta}_j)] - \ln[V] \quad (20)$$

where $V_j(\mathbf{x}, \mathbf{\Theta}_j)$ is the capacity in the jth mode of failure and V (defined earlier as the horizontal force acting on the wall) is the corresponding demand, we can express the fragility of the wall for the jth mode of failure as

$$F_j(V, \mathbf{\Theta}_j) = P[\{g_j(\mathbf{x}, \mathbf{\Theta}_j) \leq 0\} | V, \mathbf{\Theta}_j] \quad (21)$$

Because the failure of the URM wall is triggered by the exceedance of the capacity in any of the three different failure modes, following Gardoni et al. (2002) we formulate the problem as a series system reliability (Ditlevsen and Madsen 1996)

$$F(V, \mathbf{\Theta}) = P[\bigcup_j \{g_j(\mathbf{x}, \mathbf{\Theta}_j) \leq 0\} | V, \mathbf{\Theta}] \quad (22)$$

Following Gardoni et al. (2002), we obtain the predictive estimate of the fragility as the expected value of $F(V, \mathbf{\Theta})$ over the posterior distribution of $\mathbf{\Theta}$, that is
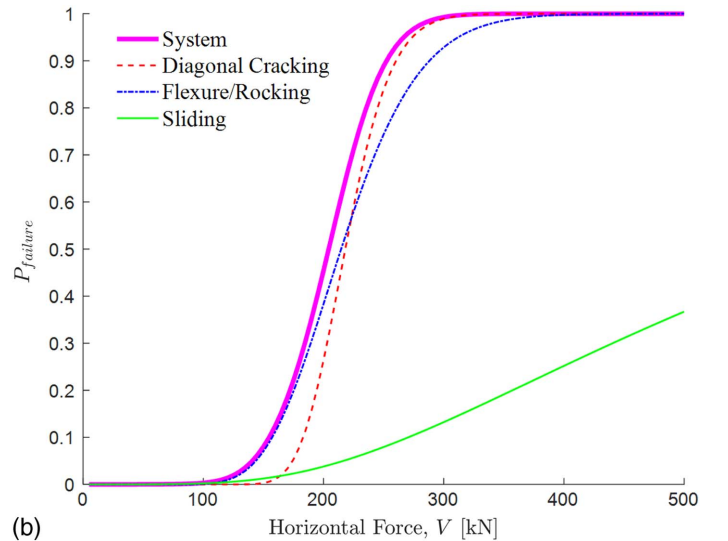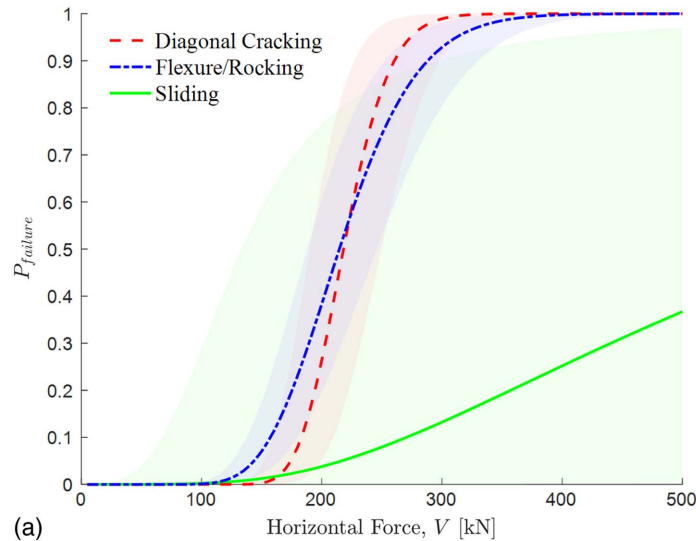
$$\tilde{F}(V) = \int F(V, \mathbf{\Theta}) f(\mathbf{\Theta}) d\mathbf{\Theta} \quad (23)$$

Finally, we can then obtain the n-standard deviations bounds for the fragility estimates as

$$\{\Phi[-\tilde{\beta}(V) - n\sigma_\beta(V)], \Phi[-\tilde{\beta}(V) + n\sigma_\beta(V)]\} \quad (24)$$

where $\tilde{\beta}(V) = \Phi^{-1}[1 - \tilde{F}(V)]$; and σ_β = standard deviation of the reliability index, obtainable with a first-order Taylor series expansion (Gardoni et al. 2002). We can obtain confidence bounds of 67%, 95%, and 99% by selecting $n = 1$, 2, and 3, respectively.
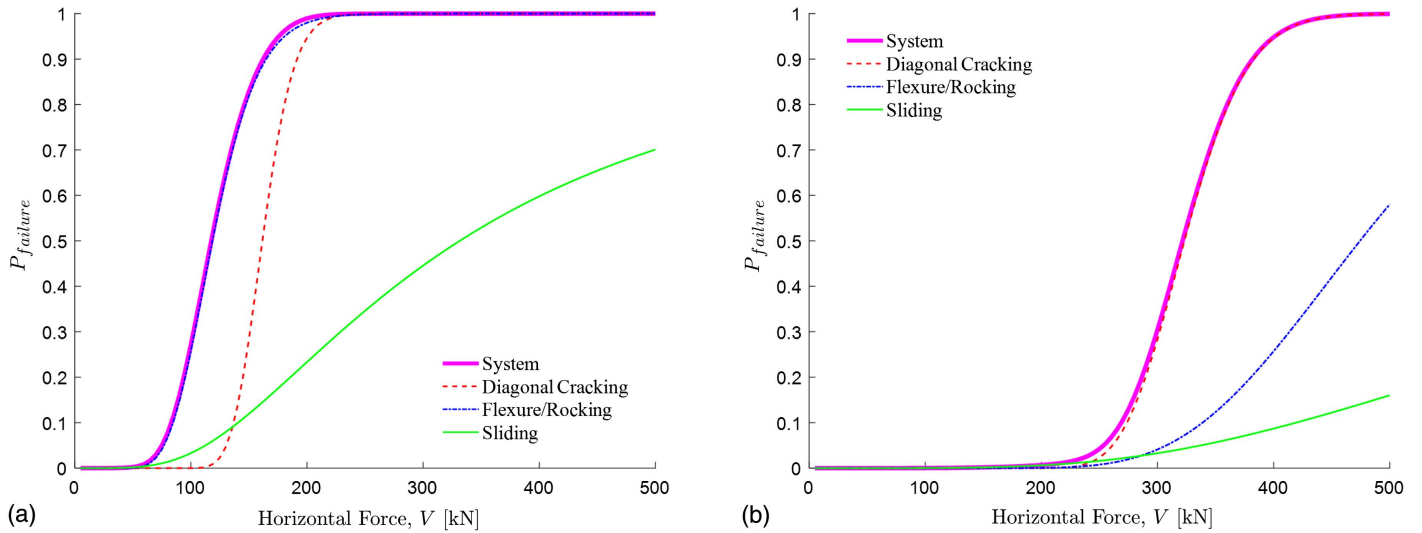
Fragility Functions for an Example of URM Wall

The models obtained in the previous sections are used to obtain fragility functions for an example URM wall. Table 9 lists the properties of the URM wall. We take geometric properties of the wall as deterministic values, while material properties and the vertical load acting on the wall are taken as lognormally distributed. The choice of a lognormal distribution is justified by Stewart and Lawrence (2007), among others, who have found that most common distributions (e.g., gamma, lognormal, Weibull) are accepted by typical statistical tests. The selected values for the coefficients of variation of URM strengths are at the low end of the typical range suggested in the literature (Li et al. 2014; McNeilly et al. 1996), and represent a design scenario with high-quality material. The value of the coefficient of variation of the vertical load depends on the type of building and occupancy (e.g., Bartlett et al. 2003), and we select 0.25 for the example URM wall.

Fig. 8(a) shows the predictive fragility functions for the different modes of failure. Flexure is the dominant mode of failure for values of V below 220 kN, while diagonal cracking dominates for larger values of V. The fragility functions are shown together with their 1σ confidence bounds, which appear as shaded areas around each curve. The bounds around the fragility function for sliding are larger than those for diagonal cracking and flexure/rocking, due to the higher statistical uncertainty associated with the sliding mode of failure (caused by the limited number of failure data in this mode). Fig. 8(b) shows the predictive fragility function of the series system along with the fragility functions for each mode.

Fig. 8. Fragility functions for the example wall: (a) individual modes of failure with associated confidence bounds; and (b) system fragility.
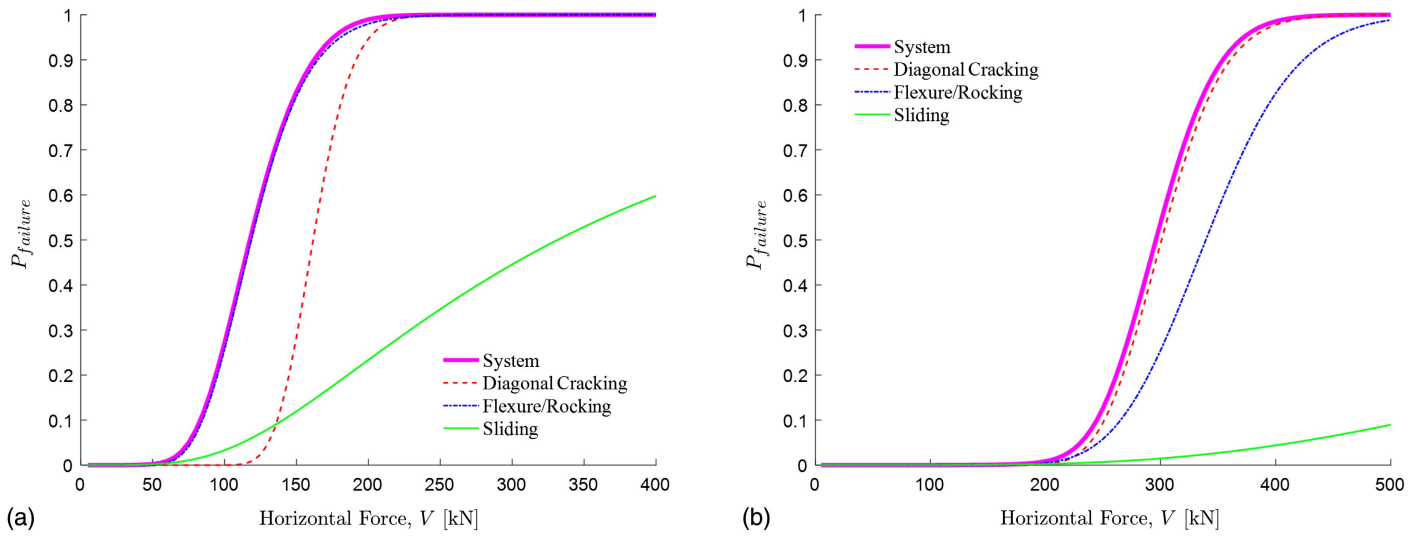
Fig. 9. Fragility functions for walls subject to (a) $N = 200$ kN; and (b) $N = 800$ kN.

Fig. 10. Fragility functions for walls with different slenderness ratios with $H = 1,500$ mm and (a) $D = 750$ mm; and (b) $D = 3,000$ mm.

The fragility function of the system coincides with the fragility function of the dominant mode of failure when there is a clear dominant mode (i.e., low and large values of V), while close to the switching point ($V = 200$ kN) the system fragility has significant contributions from both the diagonal cracking and the flexure/rocking modes of failure.

We can use the fragility functions to investigate the effect of selected variables on the failure of the URM wall. Next, we investigate the effect of the vertical load and slenderness ratio.

Effect of Vertical Load

Fig. 9 shows the fragility functions for $N = 200$ and 800 kN (the rest of the variables are kept at the values in Table 9 and Fig. 8). As anticipated, the curve for flexure lies above the curve for diagonal cracking when the vertical load is lowered to 200 kN, while the opposite is true when the vertical load is increased to 800 kN. This is in agreement with experimental and field results (Tomaževič 2009) as it highlights the predominance of flexure/sliding failures for low levels of vertical loads (e.g., upper stories of buildings) and

of diagonal cracking failures for high levels of vertical loads (e.g., lower stories of buildings).

Effect of Slenderness Ratio

We investigate the effect of the slenderness ratio of the wall, H/D, by considering $D = 750$ and 3,000 mm. The results are shown in Fig. 10. The flexural mode of failure is dominant for the more slender wall ($D = 750$ mm), while the diagonal cracking prevails for the less slender wall ($D = 3,000$ mm). The results are likely due to the different redistribution of the stresses that occur in the walls. For slender walls, the flexure/rocking failure is more likely to be initiated by cracks in the mortar on the side under tensile stress. For less slender walls, instead (particularly when $H/D < 1$) the creation of a compressed strut is likely. This can create a redistribution of internal forces which reduces the tensile stresses at the corner, and the expected failure becomes the diagonal cracking (consistently with the diagrams in Fig. 1). Due to the presence of a moderate vertical load ($N = 400$ kN), sliding never appears to be the prevalent mode of failure for these cases.

Conclusions

The paper developed new probabilistic models and fragility estimates for unreinforced masonry walls subject to in-plane horizontal forces. The models are for three possible modes of failure: diagonal cracking, flexure/rocking, and sliding. The models were constructed by adding correction terms to existing equations in the design code. The correction terms are linear combinations of a set of explanatory functions that include important physical variables for the walls. We calibrated the proposed models with a Bayesian approach using a set of experimental data from the literature. The explanatory functions were selected from a list of candidates using a stepwise deletion process. The selected explanatory functions highlight the influence of physical variables either not included or not properly accounted for in the code equations, suggesting possible revisions of the code equations. In particular, the properties of the units (such as the percentage of holes and aspect ratio) are found to play a role on the capacity of the walls. The new probabilistic models correct the bias in the original models and provide more accurate predictions. The probabilistic models also provide boundaries for the predictions.

The probabilistic models were then used to develop fragility functions for an example unreinforced masonry wall conditioning on the horizontal in-plane force. Fragility functions were developed for each failure mode considered individually and all failure modes considered in a series system. In the fragility analysis a distinction was made between the effects of the uncertainty in the input variables (e.g., geometric properties, boundary conditions, strength parameters) and the statistical uncertainty from the variability in the model parameters. The developed fragility functions can be integrated with a seismic demand model for the horizontal in-plane force to obtain seismic fragility functions conditioned on a measure of seismic load.

References

Abrams, D. P. 2001. "Performance-based engineering concepts for unreinforced masonry building structures." *Prog. Struct. Mater. Eng.* 3 (1): 48–56. https://doi.org/10.1002/pse.70.

Abrams, D. P., and N. Shah. 1992. *Cyclic load testing of unreinforced masonry walls*. No. ACTC-92-26-10. Champaign, IL: Univ. of Illinois at Urbana–Champaign.

Andreini, M., A. De Falco, L. Giresini, and M. Sassu. 2014. "Structural damage in the cities of Reggiolo and Carpi after the earthquake on May 2012 in Emilia Romagna." *Bull. Earthquake Eng.* 12 (5): 2445–2480. https://doi.org/10.1007/s10518-014-9660-7.

Anthoine, A. 1995. "Derivation of the in-plane elastic characteristics of masonry through homogenization theory." *Int. J. Solids Struct.* 32 (2): 137–163. https://doi.org/10.1016/0020-7683(94)00140-R.

Bartlett, F. M., H. P. Hong, and W. Zhou. 2003. "Load factor calibration for the proposed 2005 edition of the national building code of Canada: Statistics of loads and load effects." *Can. J. Civ. Eng.* 30 (2): 429–439. https://doi.org/10.1139/l02-087.

Benedetti, D., and G. M. Benzoni. 1984. "A numerical model for seismic analysis of masonry buildings: Experimental correlations." *Earthquake Eng. Struct. Dyn.* 12 (6): 817–831. https://doi.org/10.1002/eqe.4290120608.

Box, G. E. P., and D. R. Cox. 1964. "An analysis of transformations." *J. R. Stat. Soc.: Ser. B (Methodol.)* 26 (2): 211–243.

Box, G. E. P., and G. C. Tiao. 2011. *Bayesian inference in statistical analysis*. Reading, MA: Addison–Wesley.

CEN (European Committee for Standardization). 2004. *Eurocode 8: Design of structures for earthquake resistance—Part 1: General rules, seismic actions and rules for buildings*. EN 1998-1. Brussels, Belgium: CEN.

CEN (European Committee for Standardization). 2005a. *Eurocode: Basis of structural design*. EN 1990. Brussels, Belgium: CEN.

CEN (European Committee for Standardization). 2005b. *Eurocode 6: Design of masonry structures—Part 1-1: General rules for reinforced and unreinforced masonry structures*. EN 1996-1-1. Brussels, Belgium: CEN.

Ditlevsen, O., and H. O. Madsen. 1996. *Structural reliability methods*. New York: Wiley.

FEMA. 1997. *NEHRP guidelines for the seismic rehabilitation of buildings*. FEMA P-273. Washington, DC: FEMA.

Frumento, S., G. Magenes, P. Morandi, and G. M. Calvi. 2009. *Interpretation of experimental shear tests on clay brick masonry walls and evaluation of q-factors for seismic design*. Pavia, Italy: IUSS Press.

Gabor, A., E. Ferrier, E. Jacquelin, and P. Hamelin. 2006. "Analysis and modelling of the in-plane shear behaviour of hollow brick masonry panels." *Constr. Build. Mater.* 20 (5): 308–321. https://doi.org/10.1016/j.conbuildmat.2005.01.032.

Gardoni, P. 2017. *Risk and reliability analysis: Theory and applications* New York: Springer.

Gardoni, P., A. Der Kiureghian, and K. M. Mosalam. 2002. "Probabilistic capacity models and fragility estimates for reinforced concrete columns based on experimental observations." *J. Eng. Mech.* 128 (10): 1024–1038. https://doi.org/10.1061/(ASCE)0733-9399(2002)128:10(1024).

Giresini, L., and M. Sassu. 2018 "An on-site teaching laboratory in a village damaged by the 2009 Abruzzo earthquake." *Frattura ed Integrita Strutturale* 12 (46): 178–189. https://doi.org/10.3221/IGF-ESIS.46.17.

Grande, E., M. Imbimbo, and E. Sacco. 2013. "Finite element analysis of masonry panels strengthened with FRPs." *Composites, Part B* 45 (1): 1296–1309. https://doi.org/10.1016/j.compositesb.2012.09.002.

Haario, H., M. Laine, A. Mira, and E. Saksman. 2006. "DRAM: Efficient adaptive MCMC." *Stat. Comput.* 16 (4): 339–354. https://doi.org/10.1007/s11222-006-9438-0.

Hendry, A. W. 1981. *Structural brickwork*. New York: Wiley.

Ignatakis, C., E. Stavrakakis, and G. Pennelis. 1989. "Analytical model for masonry using the finite element method." In *Structural repair and maintenance of historical buildings*, edited by C. A. Brebbia, 511–523. Southampton, Basel: Computational Mechanics Publications.

Lagomarsino, S., and S. Cattari. 2014. "Fragility functions of masonry buildings." In *Syner-G: Topology definition and fragility functions for physical elements at seismic risk*, 111–156. Dordrecht, Netherlands: Springer.

Li, J., M. J. Masia, M. G. Stewart, and S. J. Lawrence. 2014. "Spatial variability and stochastic strength prediction of unreinforced masonry walls in vertical bending." *Eng. Struct.* 59: 787–797. https://doi.org/10.1016/j.engstruct.2013.11.031.

Lourenço, P. B. 2002. "Computations on historic masonry structures." *Prog. Struct. Mater. Eng.* 4 (3): 301–319. https://doi.org/10.1002/pse.120.

Lourenço, P. B., J. G. Rots, and J. Blaauwendraad. 1994. "Implementation of an interface cap model for the analysis of masonry structures." In *Proc., European Conf. on Computational Modelling of Concrete Structures*. Swansea, UK: Pineridge Press.

Magenes, G., and G. M. Calvi. 1997. "In-plane seismic response of brick masonry walls." *Earthquake Eng. Struct. Dyn.* 26 (11): 1091–1112. https://doi.org/10.1002/(SICI)1096-9845(199711)26:11<1091::AID-EQE693>3.0.CO;2-6.

Marques, R., and P. B. Lourenço. 2011. "Possibilities and comparison of structural component models for the seismic assessment of modern unreinforced masonry buildings." *Comput. Struct.* 89 (21–22): 2079–2091. https://doi.org/10.1016/j.compstruc.2011.05.021.

McNeilly, T., J. Scrivener, S. Lawrence, and S. Zsembery. 1996. "A site survey of masonry bond strength." *Aust. Civ. Eng. Trans.* 38 (2/3/4): 103.

Mengi, Y., and H. G. McNiven. 1989. "A mathematical model for the in-plane non-linear earthquake behaviour of unreinforced masonry walls. Part 1: Experiments and proposed model." *Earthquake Eng. Struct. Dyn.* 18 (2): 233–247. https://doi.org/10.1002/eqe.4290180208.

Morandi, P., L. Albanesi, F. Graziotti, T. L. Piani, A. Penna, and G. Magenes. 2018. "Development of a dataset on the in-plane experimental response of URM piers with bricks and blocks." *Constr. Build. Mater.* 190: 593–611. https://doi.org/10.1016/j.conbuildmat.2018.09.070.

Murphy, C., P. Gardoni, and C. E. Harris. 2011. "Classification and moral evaluation of uncertainties in engineering modeling." *Sci. Eng. Ethics* 17 (3): 553–570. https://doi.org/10.1007/s11948-010-9242-2.

NTC (Norme Tecniche per le Costruzioni). 2018. *Decreto del ministero delle infrastrutture, supplemento ordinario n.8 alla gazzetta ufficiale n. 42 della Repubblica Italiana*. Rome: NTC.

Page, A. W. 1978. "Finite element model for masonry." *J. Struct. Div.* 104 (8): 1267–1285. https://doi.org/10.1061/JSDEAG.0004969.

Penna, A., S. Lagomarsino, and A. Galasco. 2014a. "A nonlinear macroelement model for the seismic analysis of masonry buildings." *Earthquake Eng. Struct. Dyn.* 43 (2): 159–179. https://doi.org/10.1002/eqe.2335.

Penna, A., P. Morandi, M. Rota, C. F. Manzini, F. Da Porto, and G. Magenes. 2014b. "Performance of masonry buildings during the Emilia 2012 earthquake." *Bull. Earthquake Eng.* 12 (5): 2255–2273. https://doi.org/10.1007/s10518-013-9496-6.

Pietruszczak, S., and X. Niu. 1992. "A mathematical description of macroscopic behaviour of brick masonry." *Int. J. Solids Struct.* 29 (5): 531–546. https://doi.org/10.1016/0020-7683(92)90052-U.

Rots, J. G. 1991. "Numerical simulation of cracking in structural masonry." *Heron* 36 (2): 49–63.

Ruiz-García, J., and M. Negrete. 2009. "Drift-based fragility assessment of confined masonry walls in seismic zones." *Eng. Struct.* 31 (1): 170–181. https://doi.org/10.1016/j.engstruct.2008.08.010.

Sorrentino, L., S. Cattari, F. da Porto, G. Magenes, and A. Penna. 2019. "Seismic behaviour of ordinary masonry buildings during the 2016 central Italy earthquakes." *Bull. Earthquake Eng.* 17 (10): 5583–5607. https://doi.org/10.1007/s10518-018-0370-4.

Stewart, M. G., and S. J. Lawrence. 2007. "Model error, structure reliability and partial safety factors for structural masonry in compression." *Masonry Int.* 20 (3): 107–116.

Stone, C. J. 1996. Vol. 19 of *A course in probability and statistics*. Belmont: Duxbury Press.

Tabandeh, A., P. Asem, and P. Gardoni. 2020. "Physics-based probabilistic models: Integrating differential equations and observational data." *Struct. Saf.* 87: 101981. https://doi.org/10.1016/j.strusafe.2020.101981.

Tomaževič, M. 1987. "Dynamic modelling of masonry buildings: Storey mechanism model as a simple alternative." *Earthquake Eng. Struct. Dyn.* 15 (6): 731–749. https://doi.org/10.1002/eqe.4290150606.

Tomaževič, M. 2009. "Shear resistance of masonry walls and Eurocode 6: Shear versus tensile strength of masonry." *Mater. Struct.* 42 (7): 889–907. https://doi.org/10.1617/s11527-008-9430-6.

Turnšek, V., and F. Čačovič. 1970. "Some experimental results on the strength of brick masonry walls." In *Proc., 2nd Int. Brick and Block Masonry Conf.* Stoke-on-Trent, UK: British Ceramic Research Association.

Turnšek, V., and P. Sheppard. 1980 "The shear and flexural resistance of masonry walls." In *Proc., Int. Research Conf. on Earthquake Engineering*. Skopje, Yugoslavia: NIGRO.

Willis, C. R., R. Seracino, and M. C. Griffith. 2010. "Out-of-plane strength of brick masonry retrofitted with horizontal NSM CFRP strips." *Eng. Struct.* 32 (2): 547–555. https://doi.org/10.1016/j.engstruct.2009.10.015.